Renewable and Sustainable Energy Reviews

Experimental investigation on the hydrodynamic performance of a multi-chamber OWC-breakwater

--Manuscript Draft--

Manuscript Number:	
Article Type:	Original Research Article
Section/Category:	Marine and Ocean Energy
Keywords:	wave energy device; oscillating water column; multiple chamber; hydrodynamic performance; experiment
Corresponding Author:	Mingwei Li Harbin Engineering University CHINA
First Author:	Xuanlie Zhao
Order of Authors:	Xuanlie Zhao
	Lidong Zhang
	Mingwei Li
	Lars Johanning
Abstract:	Multi-chamber Oscillating Water Column (OWC) device have recently become more attractive due to its potential high efficiency. In this paper, the hydrodynamic performance of a single-, dual- and triple-chamber OWC breakwater are investigated experimentally. In the first instance quantitative comparisons are conducted to understand the hydrodynamics of the multi-chamber -OWC-breakwater. Specific attention has been dedicated to the hydrodynamic performance of capture width ratio (CWR), reflection coefficient, transmission coefficient, dissipation coefficient and effective frequency bandwidth. The investigation identified various findings that are summarized in the following: i) it was found that the maximum CWR increases with increasing chamber number n (i.e., n = 1, 2, 3), if the volume of the combined water columns was kept the same; ii) in longer waves the triple-chamber OWC-breakwater showed better performance, within an increase in capture bandwidth, that satisfied the condition of $K_T < 0.5$ and $\eta > 20\%$; iii) it was found that the multiple-chamber OWC device has improved wave energy extraction characteristics at high frequency region; iv) positive hydrodynamic interactions between the different columns improved the performance of the multiple-chamber OWC-breakwater device; v) wave nonlinearity is important for evaluating the performance of the multiple-chamber OWC-breakwater device; and vi) for the triple-chamber OWC device the dissipation coefficient increases as wave nonlinearity increases, whilst the CWR and the transmission coefficient decrease over the range of wave frequencies investigated.
Suggested Reviewers:	Rongquan Wang Dalian University of Technology rqwang@dlut.edu.cn wave energy utilization, wave-structure interaction
	George Aggidis Lancaster University Renewable Energy Group g.aggidis@lancaster.ac.uk
	Ahmed Elhanafi University of Tasmania Ahmed.Elhanafi@utas.edu.au
	Fang He Zhejiang University hefang@zju.edu.cn
Opposed Reviewers:	

Experimental investigation on the hydrodynamic performance of a multi-chamber OWC-breakwater

Xuanlie Zhao[1], Lidong Zhang[1], Mingwei Li[1*], Lars Johanning[1,2]

1.College of Shipbuilding Engineering, Harbin Engineering University, Harbin, 150001, China

2.College of Engineering, Mathematics and Physical Sciences, Exeter University, Cornwall TR10 9FE, UK

Abstract

Multi-chamber Oscillating Water Column (OWC) device have recently become more attractive due to its potential high efficiency. In this paper, the hydrodynamic performance of a single-, dual- and triple-chamber OWC breakwater are investigated experimentally. In the first instance quantitative comparisons are conducted to understand the hydrodynamics of the multi-chamber -OWC-breakwater. Specific attention has been dedicated to the hydrodynamic performance of capture width ratio (*CWR*), reflection coefficient, transmission coefficient, dissipation coefficient and effective frequency bandwidth. The investigation identified various findings that are summarized in the following: i) it was found that the maximum *CWR* increases with increasing chamber number n (i.e., n = 1, 2, 3), if the volume of the combined water columns was kept the same; ii) in longer waves the triple-chamber OWC-breakwater showed better performance, within an increase in capture bandwidth, that satisfied the condition of K_T < 0.5 and η > 20%; iii) it was found that the multiple-chamber OWC device has improved wave energy extraction characteristics at high frequency region; iv) positive hydrodynamic interactions between the different columns improved the performance of the multiple-chamber OWC-breakwater device; v) wave nonlinearity is important for evaluating the performance of the multiple-chamber OWC-breakwater device; and vi) for the triple-chamber OWC device the dissipation coefficient increases as wave nonlinearity increases, whilst the *CWR* and the transmission coefficient decrease over the range of wave frequencies investigated.

Keywords: wave energy device; oscillating water column; multiple chamber; hydrodynamic

[*] Corresponding author (limingwei@hrbeu.edu.cn)

performance; experiment

1 Introduction

With the exhaustion of fossil fuel resources and its environmental impacts on climate change and air pollution, renewable energy resources have become attractive, providing increasingly a sustainability energy alternative [1]. Offshore Renewable Energy (ORE)resources have gained wide attention, especially the commercialization of offshore wind, but also other ocean energy resources such as wave energy, tidal energy and thermal energy have gained large attention [2]. Wave energy has the advantages of large reserves, diverse geographical distribution and huge potential [3]. Many theoretical studies on wave energy devices have been conducted since 1970s. In the following decades, many experimental and numerical studies have been widely performed. To date, a fast amount of wave energy converters have been patented and many concepts are at a stage of sea trial [4]. Based on the working principle, wave energy devices can be classified as point absorber, terminator or attenuator in form of Oscillating Water Column (OWC), oscillating body, and overtopping type [4].

OWC wave energy devices extract energy through an air flow generated by the rise and fall in wave crest in a chamber. The OWC technology has seen significant research addressing efficiency, best turbine design, survivability, etc. for onshore and offshore applications [5]. Theoretical, numerical and experimental studies proved that this kind of devices have great prospects in the field of wave energy extraction [6-14]. There are also various OWC devices that are at field trial, such as the Mutriku OWC breakwater [15], Resonant Wave Energy Converter 3 (REWEC3) [16-17], LIMPET device, etc. Integrating an OWC device into a breakwater has been discussed to be attractive due to the cost and space sharing [18-19]. However, the economic viability of OWCs are is currently low as a result of wave energy conversion efficiency and high cost. The integrations of WECs into breakwaters provides potentially the opportunity to enhance the economic viability of OWC WECs that needs further efficiency enhancement to make this technology commercially viable. Enhancing the energy conversion efficiency of OWCs could be achieved through PTO control strategy, array layout of the devices and modification of the device geometry [20-21]. Although many interesting improvements have been achieved, further investigations improving the efficiency are essential. In this paper, the focus is on the multi-chamber OWC device.

Extensive investigations have been conducted on multi-chamber OWC devices. Hsieh et al.[22] presented the laboratory test on energy capture performance of a floating dual-chamber OWC device. Experimental data showed that the dual-chamber design can improve the overall power generation, and the output can be smoothed since the two chambers work out of phase. Martinelli et al.[23] investigated the performance of a multi-chamber Seabreath OWC device that has four chambers. They point out that the maximum efficiency occurs when the wavelength is equal to the chamber length. Rezanejad et al.[24] investigated the hydrodynamic characteristics of the shoreline-based dual-chamber OWC device over a stepped bottom. Theoretical results showed that the efficiency of the dual-chamber OWC device is greater then that of the single-chamber device. It was shown that the stepped bottom has a significant effect on the investigated OWC efficiency. Ning et al.[25] presented a parametric study on the shoreline-based dual-chamber OWC device. In this study a simplified PTO system was configured in the dual-chamber device. Ning et al.[26] further investigated the shoreline-based dual-chamber system using experimental methods. The sensitivity of the various parameters on the efficiency were analyzed and the valuable experimental data were documented.

Iturrioz et al.[27] developed a numerical time-domain tool for predicting the hydrodynamic performance of a fixed OWC device as a first step towards modelling a floating multi-chamber OWC device. The time domain model was developed using Cummins method and the model was verified by comparing the numerical study with experimental results and a CFD study. He et al.[28] studied two individual OWC chambers integrated into a floating breakwater. A thorough hydrodynamic performance was explored using experimental study. The results showed that an asymmetric configuration of the chambers lead to a larger air pressure, enhancing the efficiency of the system. Following this study, He et al. [29] investigated the power extraction performance of the floating breakwater with dual OWC chambers. This study concluded that the natural frequency of the two chambers has an effect on capture bandwidth. Howe et al. [30] investigated the energy extraction, wave attenuation performance and motion characteristics of a floating breakwater with multiple chambers. The study identified that the hydrodynamic interactions of the chambers significantly affects the hydrodynamic performance of the system.

Elhanafi et al.[31] examined numerically the performance of a floating dual-chamber device, focusing on a comparison with a single-chamber device. The study supports the work by Rezanejad et al.[24], stating that the efficiency can be significantly improved using a dual–chamber system. Ning et al.[32] proposed a novel cylindrical dual-chamber OWC device and implemented a theoretical study. The investigation discovered the presence of three free-surface oscillation modes in the chamber. In order to support this theoretical finding, Ning et. al. [33] followed up with an experimental study and observed the existence of two different resonant frequencies corresponding to the inner- and outer-chambers, and concluded that the combination of the two different resonant frequencies of inner and outer chambers lead to a wider frequency region. Shalby et al.[34-35] proposed a new type of MC-OWC wave energy device, which has four chambers along the incident wave direction. Numerical 3-D studies with focus on the capture width ratio and free surface elevation were presented. It was found that the increased incident wave height reduces the device efficiency.

In this paper, we aim to investigate the hydrodynamic performance of the floating multi-chamber OWC device by considering the function of wave energy extraction and breakwater. In this paper, we call this kind of device with both functions as the OWC-breakwater. The contribution to knowledge of the present paper is the direct experimental comparisons of the single-, dual- and triple-chamber OWC-breakwater that will be discussed comprehensively. The work described here will provide the research community with an in-depth understanding of the hydrodynamic performance of the multi-chamber OWC-breakwater integrated in a floating breakwater. The paper is organized as follows: firstly a description of the experimental set-up will be discussed and data will be presented in Section 2; In Section 3 the results will be presented and discussed; and finally a conclusions will summarize the findings in Section 4.

2 Experiment description

2.1 Experimental setup

The physical tests were carried out in a wave flume at Harbin Engineering University, China (see Figure 1). The dimensions of the wave flume are as follows: length 33.0 m, width

0.8 m and depth 1.0 m. The flume is equipped with a piston-type wave maker and a wave-absorbing beach. The data acquisition and processing system consists of wave gauge, pressure sensor, data acquisition instrument and data processing system. The wave gauges and pressure sensors were carefully calibrated over a range from zero to 40mm at a step of 0.4mm and zero to 10kPa at a step of 10Pa, respectively. The data were collected using a specific data acquisition processing system.

Figure 1. Photo of the wave flume.

The physical model tests were carried out using the scale of 1:20 applying Froude scaling. The water depth h was set as 0.60 m, the wave height was selected as H_i = 0.05 m, 0.075 m and 0.10 m, and the experimental wave periods T varies from 1.1 s to 1.8 s at interval of 0.1 s. The combination of test cases is presented in Table 2.

In order to decrease the influence of the flume side wall on the experimental investigations, the OWC models width, perpendicular to the incident wave direction, was set as 0.78 m. The details of the single-, dual- and triple-chamber design are presented in Table 1 and supported by Figure 2(a-c) and 3(a-c). The models were manufactured from 10 mm thick Perspex sheets. The opening ratios of single-chamber OWC-breakwater are 0%, 0.5%, 1.0%, 1.5%, 2.0% and 25% (as shown in Table 1. The effect of PTO damping on device performance was investigated by changing the opening ratio [26, 29, 36]. Symmetric PTO damping of dual-chamber model is discussed to be more effective than the asymmetric PTO damping [31]. As a consequence, each chamber was equally divided and the opening ratio were kept the same for the dual- and triple-chamber OWC-breakwater. The opening ratios of dual-chamber OWC-breakwater are 0%, 1.0% and 1.5%, and for the triple-chamber OWC-breakwater are 0%, 1.0%, 1.5% and

15.8%. In the literature it is suggested that an opening ratio > 4.03% results in a very low power extraction and that the pressure fluctuations of the each chamber can be negligible [37]. Hence, we regard the cases of 15.8% and 25% as the fully opened case. The specific dimensions and numbers of the physical models are shown in Table 1.

Table 1 The specific dimensions of the physical models.

physical models	length（m）	width（m）	height（m）	No.	opening ratio	dimensions（mm）
single-chamber OWC-breakwater	0.78	0.62	0.99	S1	0%（fully closed）	—
				S2	0.5%（orifice）	54
				S3	1.0%（orifice）	76
				S4	1.5%（orifice）	93
				S5	2.0%（orifice）	108
				S6	25%（slot, perpendicular to the incident wave direction）	150
dual-chamber OWC-breakwater	0.78	0.63	0.99	D1	0%（fully closed）	—
				D2	1.0%（orifice）	54
				D3	1.5%（orifice）	66
triple-chamber OWC-breakwater	0.78	0.64	0.99	T1	0%（fully closed）	—
				T2	1.0%（orifice）	44
				T3	1.5%（orifice）	54
				T4	15.8%（slot, parallel to the incident wave direction）	120

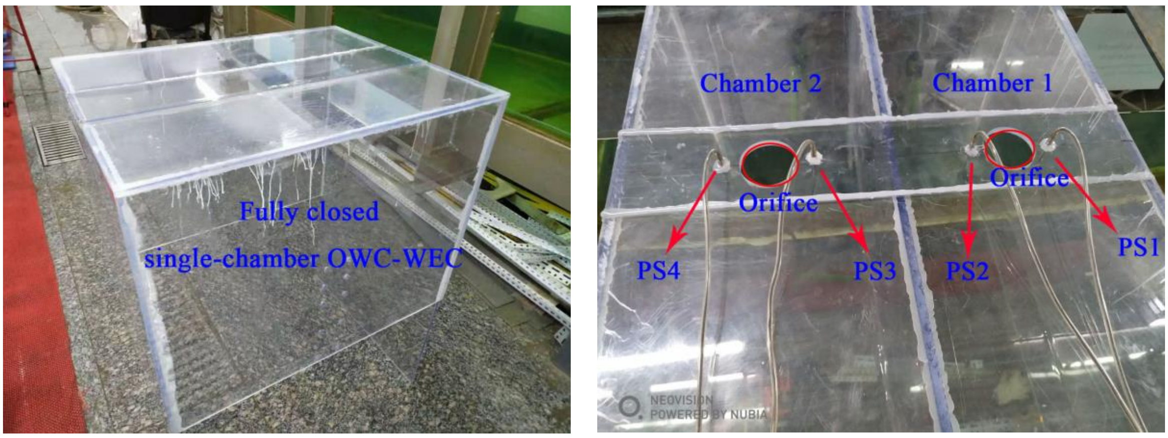

(a) (b)

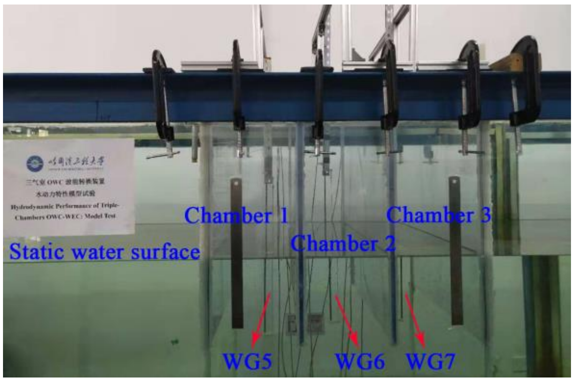

(c)

Figure 2. Photos of physical models. WG: wave gauge, PS: pressure sensor.

The models were installed at 19.0 m away from the wave maker with a fixed draft of 0.2 m. Four wave gauges were installed at the weather side (WG1 & WG2) and leeside (WG3 & WG4) of the OWC-breakwater monitoring incident wave, as well as the reflected and transmitted waves. Furthermore, wave gauge WG5, WG6 and WG7 were placed in the center of the chamber(s) (single-, dual-, triple chamber configuration) as shown in Figure 3(a-c). In addition to placing a wave gauge into each chamber, two pressure sensors were also installed close to the edge of the orifice. Figure 3(a) shows location of pressure gauges for the single chamber (PS1 & PS2), Figure 3(b) for the dual chamber (PS1 & PS2 and PS3 & PS4), and Figure 3(c) for triple chamber (PS1 & PS2, PS3 & PS4 and PS5 & PS6).

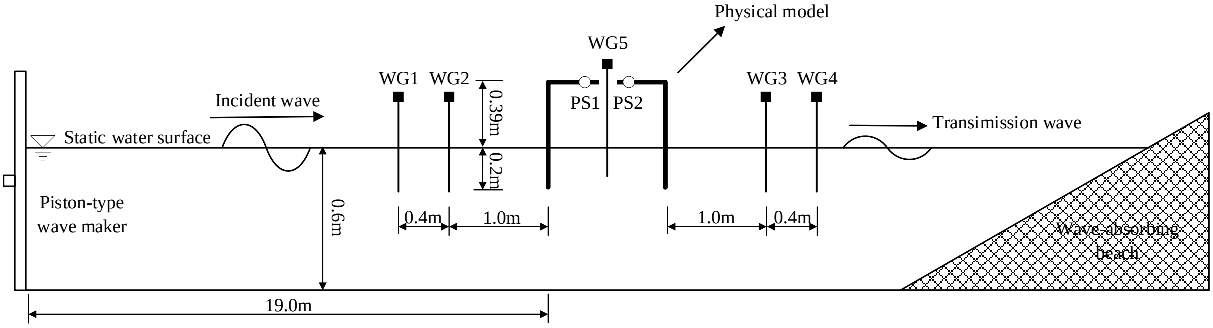

(a)

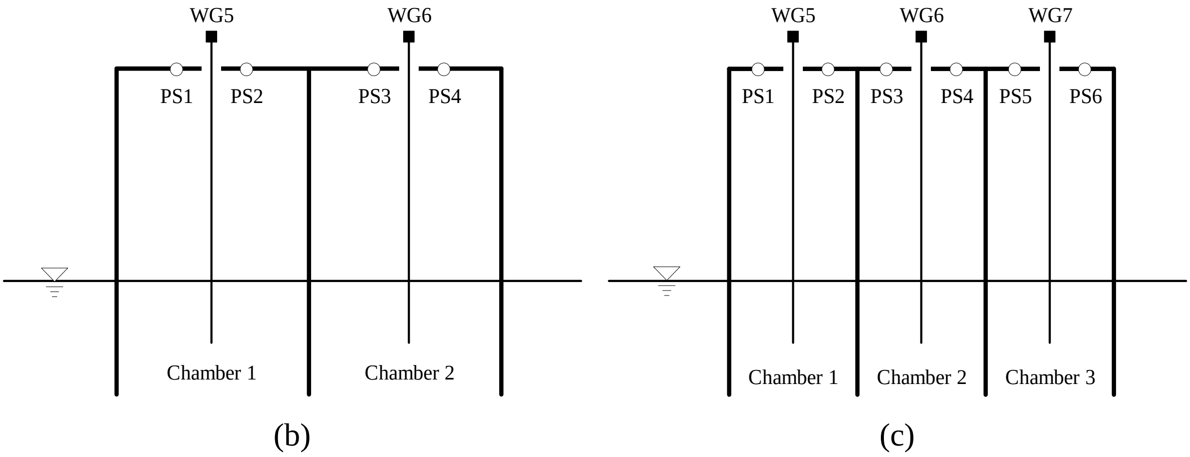

Figure 3. Experimental set-up (a) and the layout of the sensors for dual- (b) and triple-chamber device (c)

2.2 Data acquisition and analysis

The combination of wave conditions and dimensionless wave number *kh* are shown in Table 2. Using the two-point method of Goda and Suzuki[38], reflected wave height H_R and transmitted wave amplitude H_T can be obtained. The reflection coefficient K_R and the transmission coefficient K_T can be calculated as H_R/H_i and H_T/H_i, respectively.

Table 2 Wave conditions.

No.	Test case	Water depth (m)	Incident wave height (m)	Wave period (s)	Dimensionless wave number *kh*
1	S1/S2/S3/S4/S5/S6	0.60	0.05	1.1/1.2/1.3/1.4/1.5/1.6/1.7/1.8	2.06/1.78/1.56/1.39/1.26/1.15/1.06/0.99
2	D1/D3/T1/T3/T4		0.05		
3	D2/T2		0.05/0.075/0.10		

The *CWR* is determined by the ratio of the power absorbed by the OWC-breakwater and the incident wave power. The averaged absorbed power of *n*th (n = 1, 2, 3) chamber is calculated as follows:

$$\bar{P}_n = \frac{B}{T}\int_{t_0}^{t_0+T}\sqrt{\frac{2\left|p_n'(t)\right|^3}{\rho_a C_f}}\mathrm{d}t \tag{1}$$

where B is the width of pneumatic chamber, T is the wave period, t_0 is some moment, $p'_n(t)$ is the air pressure fluctuation inside the nth (n =1, 2, 3) chamber; ρ_a is the air density, the quadratic coefficient $C_f = (\frac{1}{\alpha C_c} - 1)^2$ [39], α is the opening ratio, the contraction coefficient

$C_c = \frac{1}{0.639(1-\alpha)^{0.5} + 1}$ [40].

The capture width ratio of each chamber η_n and the total CWR are calculated as $\eta_n = \overline{P}_n / P_i$ and $\eta = \sum_{i=1}^{n} \eta_n$, respectively. For the single-chamber device, the total CWR is $\eta = \eta_1$. The incident wave power with per unit width is $P_i = \frac{1}{8}\rho_w g H_i^2 \frac{\omega}{2k}(1 + \frac{2kh}{\sinh 2kh})$, where ρ_w is the water density, g is acceleration due to gravity, C_g is the velocity of wave group, ω is the wave angular frequency.

According to the energy conservation law, the dissipation coefficient K_D is calculated by $K_D = 1 - K_R{}^2 - K_T{}^2 - \eta$.

The air pressure fluctuation $p'_n(t)$ inside the nth (n =1, 2, 3) chamber at a certain time is calculated by the average of two pressure sensors near the orifice. The detailed calculations of $p'_n(t)$ can be written as $p'_1(t) = (p_1(t) + p_2(t))/2$, $p'_2(t) = (p_3(t) + p_4(t))/2$ and $p'_3(t) = (p_5(t) + p_6(t))/2$ .The results of the contraction coefficient C_c and quadratic coefficient C_f of the OWC-breakwater at different opening ratios are shown in Table 3.

Table 3 Contraction coefficient C_c and quadratic coefficient C_f of the OWC devices.

opening ratio α	0.5%	1.0%	1.5%	2.0%
C_c	0.6017	0.6113	0.6119	0.6125
C_f	106589	26432	11652	6501

3 Results and discussion

3.1 Hydrodynamic performance of the single-chamber OWC-breakwater

In this section, we investigated and compare the hydrodynamic performance of the single-chamber and dual-chamber including parameters such as wave elevation and air pressure fluctuation in the chamber, capture width ratio, reflection coefficient, transmission coefficient, dissipation coefficient and effective frequency bandwidth. The related hydrodynamic parameters of OWC-breakwaters are shown in Table 4. Both the *CWR* and the transmission coefficient are important in the evaluation of the performance of the OWC-breakwaters integrated into a breakwater. A further parameter that need consideration is the effective frequency bandwidth, required to study the *CWR* and transmission coefficient. The test cases (see Table 1) for the single-chamber device are S1, S2, S3, S4, S5 and S6 and for the dual-chamber OWC-breakwater are D1, D2 and D3. For these cases the incident wave height was fixed at 0.05 m and the wave periods T vary from 1.1s to 1.8s at an interval of 0.1s.

Table 4 Hydrodynamic parameters of OWC-breakwaters.

parameters	definition
ζ	free surface elevation
A	first order wave amplitude
ΔP	amplitude of air pressure fluctuation
η	capture width ratio
K_R	reflection coefficient
K_T	transmission coefficient
K_D	dissipation coefficient

3.1.1 Capture width ratio

In the first instance the hydrodynamic performance of the single-chamber OWC-breakwater for various wave periods and opening ratios are discussed to understand the hydrodynamic characteristics and enable the comparison to the dual-chamber device. For this the wave elevation and the air pressure fluctuation in the single chamber was investigated. A spectral frequency analysis was performed on the time-history of the free surface elevation within the chamber（WG5）that is shown in Figure 4. Initially the repeatability was assessed comparing the spectrum of two different test runs. Furthermore, the spectrum was used to analyze the dominant and secondary and third order wave frequencies occurring within the chamber.

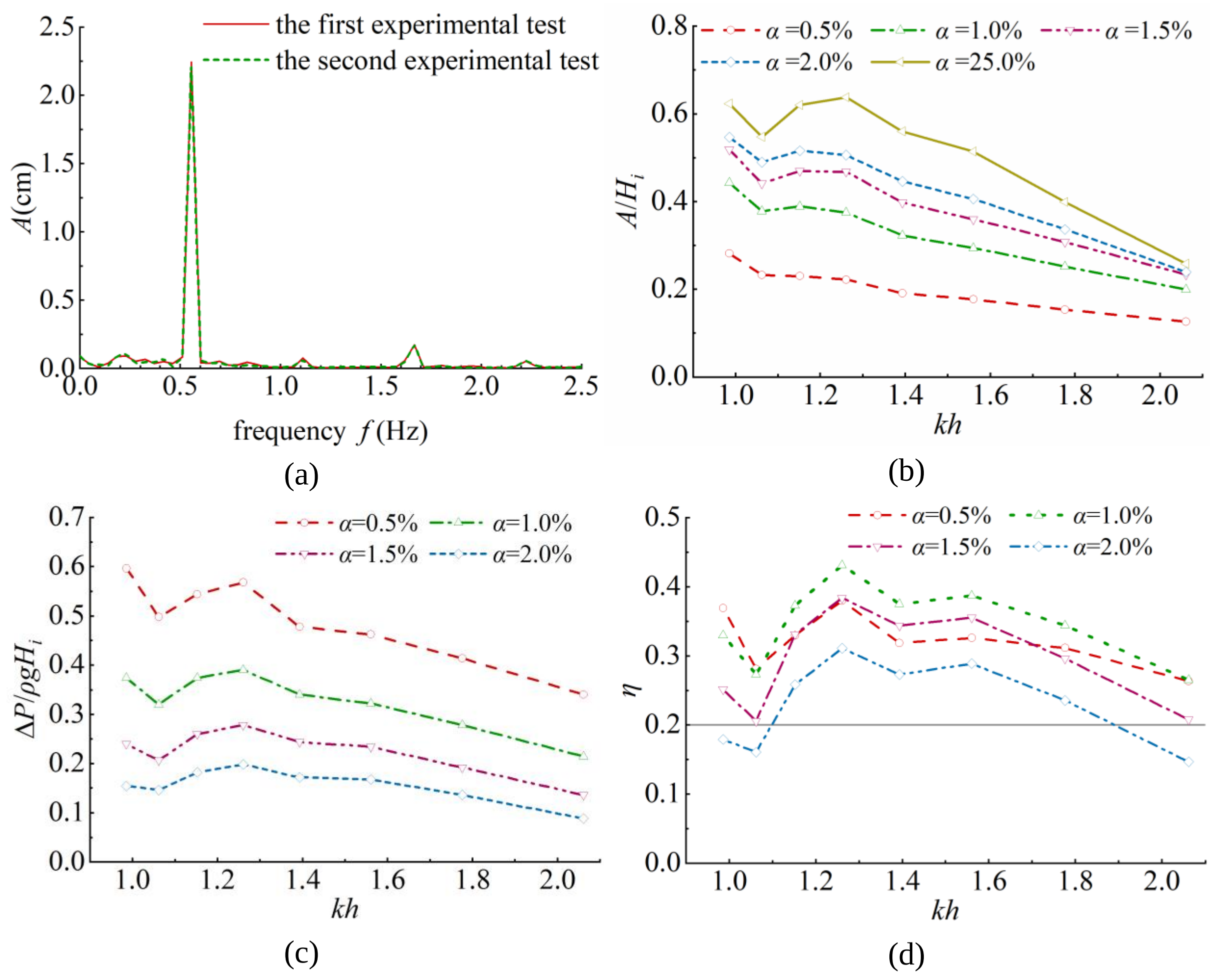

Figure 4. Spectral frequency analysis of the free surface elevation in the chamber (a) and the results of the relative wave amplitude A/H_i (b), relative amplitude of air pressure fluctuation $\Delta P/\rho g H_i$ (c), and CWR η (d) for the single-chamber OWC-breakwater.

Figure 4(b) shows results of the first-order wave amplitude. It can be seen that the relative wave amplitude A/H_i increases with an increasing opening ratio α. The relative wave amplitude exhibits an initial step drop followed by an increase in values before a steady drop can be observed. This is mainly reflected in that an obvious dip in value was observed at the lower frequency region (kh =1.06).

Figure 4(c) plots the trend of relative amplitude of air pressure fluctuation $\Delta P/\rho gH_i$ against kh in different opening ratios. The amplitude of air pressure fluctuation ΔP was calculated as the average of air pressures measured by the two pressure sensors located at the air hole (i.e., $\Delta P= (\Delta p_1+\Delta p_2)/2$). A similar behavior as in Figure 4(b) can be observed with air pressure fluctuations dropping at kh =1.06 for all cases, but at different severity. Specially, the relative amplitude of air pressure fluctuation at the lower frequency ration (i.e., kh = 0.99) is greater than that of the peak value for α = 0.5%. The increasing of the opening ratio reduces the relative amplitude of air pressure fluctuation.

As for *CWR*, the same trend was found at kh=1.06. The location of the dip in value of *CWR* is the same as that for the relative amplitude of air pressure fluctuation in Figure 4(c) (ω = 4.19rad/s). And, as kh increases, the efficiency approaches to the peak value at kh=1.26. After that, the *CWR* exhibits a monotonically decreasing trend. It is found that the *CWR* maximum approaches to 43.1% when α = 1.0%. Due to the influence of the viscosity dissipation, the maximum *CWR* cannot approach to the theoretical value of 50% in case of the symmetrical chamber wall [47].

In addition, we observe that the optimal opening ratio increases with increasing wave periods for different frequency region. Detailly, the optimal opening ratios for frequency range of 0.99 < kh < 1.06 and 1.06 < kh < 2.06 are α=0.5% and α=1.0%, respectively.

3.1.2 Reflection coefficient and transmission coefficient

Reflection coefficient and the transmission coefficient are the important factors while evaluating the performance of the OWC-breakwater. In this subsection, we investigate the reflection coefficient and transmission coefficient of the single-chamber OWC-breakwater.

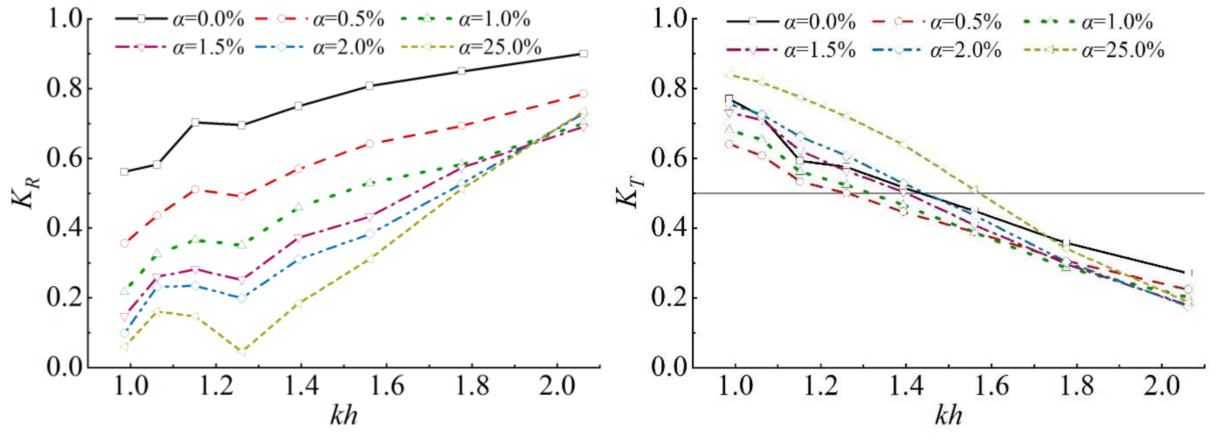

(a) (b)

Figure 5. Variations of reflection (a) and transmission coefficient (b) of single-chamber OWC-breakwater with *kh* in different opening ratios.

Figure 5 shows the results of reflection coefficient and transmission coefficient of the single-chamber OWC-breakwater for various wave periods and opening ratios. The reflection coefficient increases with the increasing *kh* with exception of the valley value at *kh* = 1.26. It is corresponding to the location of the peak value of the *CWR* shown in Figure 4(d). As for the effect of the opening ratios, the trend of K_R *vs* α is different for different frequency regions. The opening ratio affect the reflection coefficient significantly at the lower frequency region, where the reflection coefficient decreases with the increasing of the opening ratio. However, slight modification of the reflection coefficient can be found at the higher frequency region. In summary, the reflection coefficient corresponding to α = 0% is larger than that corresponding to α > 0% for the single-chamber OWC-breakwater.

From Figure 5(b), it can be found that the transmission coefficient of single-chamber OWC-breakwater monotonically decreases with increasing *kh*. For the tested opening ratios, K_T decreases firstly and then increases with the increasing opening ratio.

3.1.3 Dissipation coefficient

Figure 6 presents the dissipation coefficient K_D that is a factor that balance the energy dissipated due to viscous effect and can be obtained through $K_D = 1 - K_R{}^2 - K_T{}^2 - \eta$. The results of dissipation coefficient of single-chamber OWC-breakwaters are shown in Figure 6.

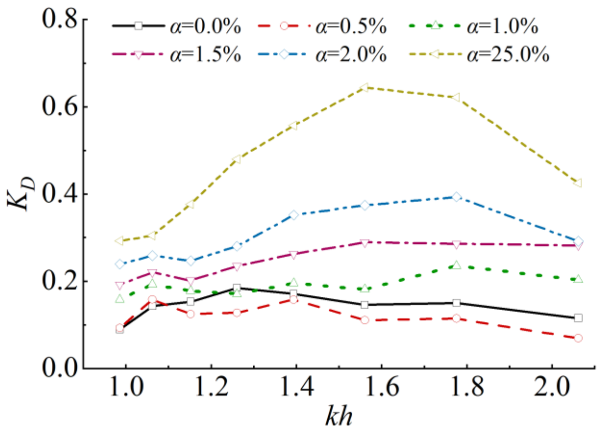

Figure 6. Variations of dissipation coefficient of single-chamber OWC-breakwater with *kh* in different opening ratios.

For the dissipation coefficient of the single-chamber OWC-breakwater, it can be observed that the dissipation coefficient increases as the opening ratio approach increases. The maximum dissipation coefficient approaches to 64.4% for case of $\alpha = 25\%$ due to the higher water particle velocity at the tip of the plate.

For the floating breakwater, the condition of $K_T < 0.5$ is often regarded as the effective transmission coefficient [56]. While for the wave energy converter, we define the condition of $\eta > 0.2$ as the satisfactory wave energy conversion device [50]. The effective frequency bandwidth is the frequency bandwidth that satisfied the condition of $K_T < 0.5$ and $\eta > 0.2$[57].

For cases of $\alpha = 0\%$, $\alpha = 0.5\%$, $\alpha = 1.0\%$, $\alpha = 1.5\%$, $\alpha = 2.0\%$ and $\alpha = 25.0\%$, the frequency ranges for $K_T < 0.5$ are $1.43 < kh < 2.06$, $1.26 < kh < 2.06$, $1.32 < kh < 2.06$, $1.40 < kh < 2.06$, $1.45 < kh < 2.06$ and $1.57 < kh < 2.06$, respectively. And, the frequency ranges for $\eta > 0.2$ are $0.99 < kh < 2.06$, $0.99 < kh < 2.06$, $0.99 < kh < 2.06$ and $1.10 < kh < 1.89$ for cases of $\alpha = 0.5\%$, $\alpha = 1.0\%$, $\alpha = 1.5\%$ and $\alpha = 2.0\%$, respectively. Hence, within the test scope, the effective frequency range corresponding to $\alpha = 0.5\%$, $\alpha = 1.0\%$, $\alpha = 1.5\%$ and $\alpha = 2.0\%$ are $1.26 < kh < 2.06$, $1.32 < kh < 2.06$, $1.40 < kh < 2.06$ and $1.45 < kh < 1.89$, respectively. Correspondingly, the effective frequency bandwidth are 1.8, 0.74, 0.66 and 0.44.

3.2 Hydrodynamic performance of dual-chamber OWC-breakwater

3.2.1 Capture width ratio

In the following the performance of the dual-chamber OWC-breakwater is examined. We tested the performance of the dual-chamber device for cases of α=0%, 1.0% and 1.5%.

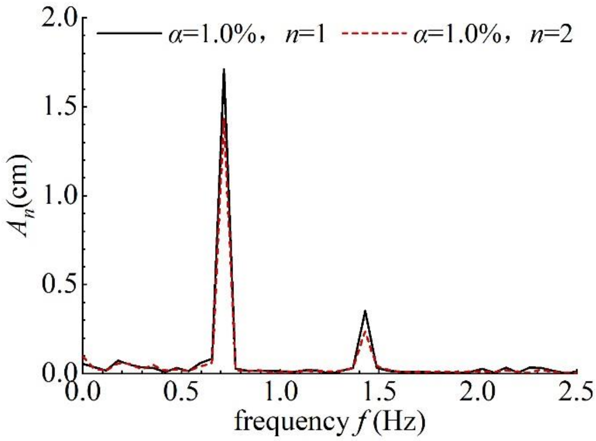

Figure 7. Spectral frequency analysis of the time-history curve of the free surface elevation (WG5, WG6) in each chamber of dual-chamber OWC-breakwater (kh = 1.39)

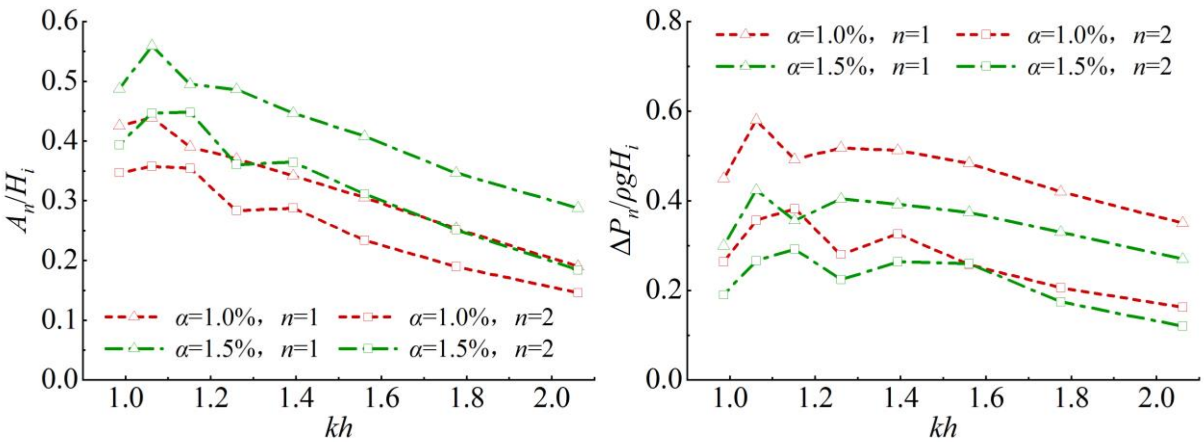

(a) (b)

Figure 8. Variations of the relative wave amplitude A_n/H_i and air pressure fluctuation $\Delta P_n/\rho g H_i$ with kh for dual-chamber OWC-breakwater

From the frequency spectral analysis shown in Figure 7, it can be found that the second-order wave amplitude is obvious compared with the first order wave amplitude when kh = 1.39.

From Figure 8(a), we found that the relative wave amplitude in the front chamber is greater than that in the rear chamber due to the shadow effect in wave propagation problems, similar phenomenon can also be found in multi-body systems [48]. Besides, the vortex shedding at the sharp edges of the wall is also one reason that can explain this phenomenon.

It is worthy to note that, for both cases of D2 (α = 1.0%) and D3 (α = 1.5%), the location of peak value for the front chamber (in Figure 8(a)) is different from that for the rear chamber. Detaily, the location of the peak value corresponding to the front chamber is less than that corresponding to the rear chamber. This is due to the hydrodynamic interactions of the two adjacent water columns in the chamber[24, 49]. Similar phenomenon for two adjacent floating bodies has been found [50].

From Figure 8(b), it was found that there are two peaks for the relative amplitude of air pressure fluctuation in each chamber. But, generally, a parabolic trend for relative amplitude of air pressure fluctuation against *kh* can be found in each case with exception of the valley value at *kh* = 1.15 and *kh* = 1.26 for the front and rear chamber, respectively.

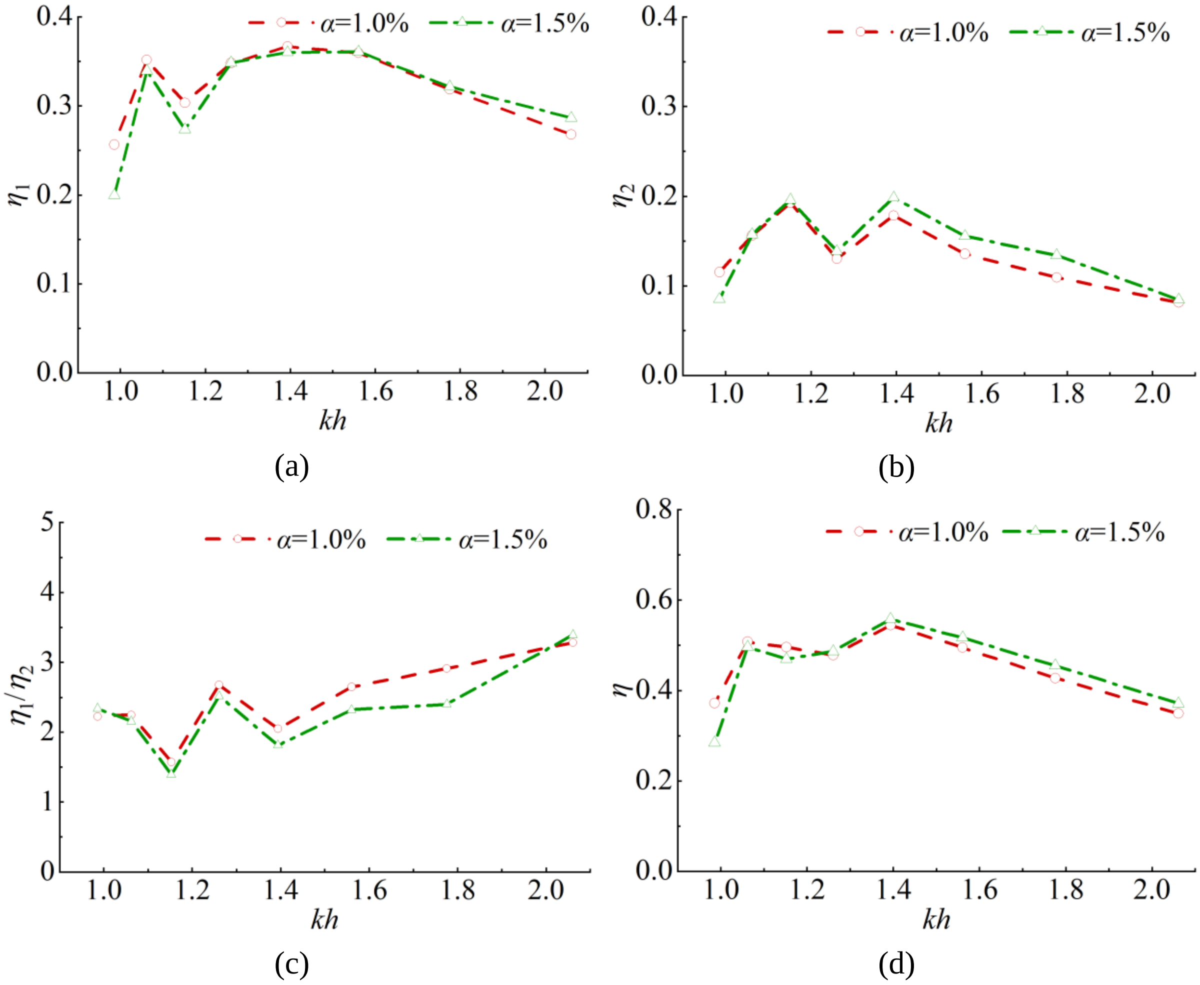

Figure 9. Variations of η_1 (a), η_2 (b), η_1/η_2 (c) and total *CWR* η(d) of dual-chamber OWC-

breakwater with *kh* in different opening ratios.

Figure 9(a-d) present results of the *CWR* in each chamber, the ratio of the *CWR* in the front chamber and the rear chamber and the total *CWR* in different opening ratios. Two spikes are observed for both the *CWR* in the front chamber and the rear chamber. This is due to the fact that the hydrodynamic interactions of two chambers lead to two resonance frequencies of two water colomns. But, the locations of the peak value of *CWR* in each chamber are different. For both cases of D2 (α = 1.0%) and D3 (α = 1.5%), the values of η_1/η_2 are always greater than 1 throughout the whole frequency region. Due to the shadow effect, the *CWR* of the front chamber is superior to that of the rear chamber. Detailly, the locations of the first spike and the second spike of η_1 are *kh*=1.06 and 1.39, respectively. For η_2, the locations of the two spikes are *kh* = 1.15 and 1.39. Note that the frequency corresponding to *kh*=1.39 (ω = 4.49rad/s) is less than that of the piston-mode natural frequency (ω = 4.98rad/s) of water column in isolated case.

From Figure 9(d), we can found that the total *CWR* for case of D2 (α= 1.0%) is close to that of the D3 (α = 1.5%). The two spikes are located at *kh*=1.06 and *kh* = 1.39. In this study, the maximum *CWR* of 55.8% can be observed for the dual-chamber system.

3.2.2 Reflection coefficient and transmission coefficient

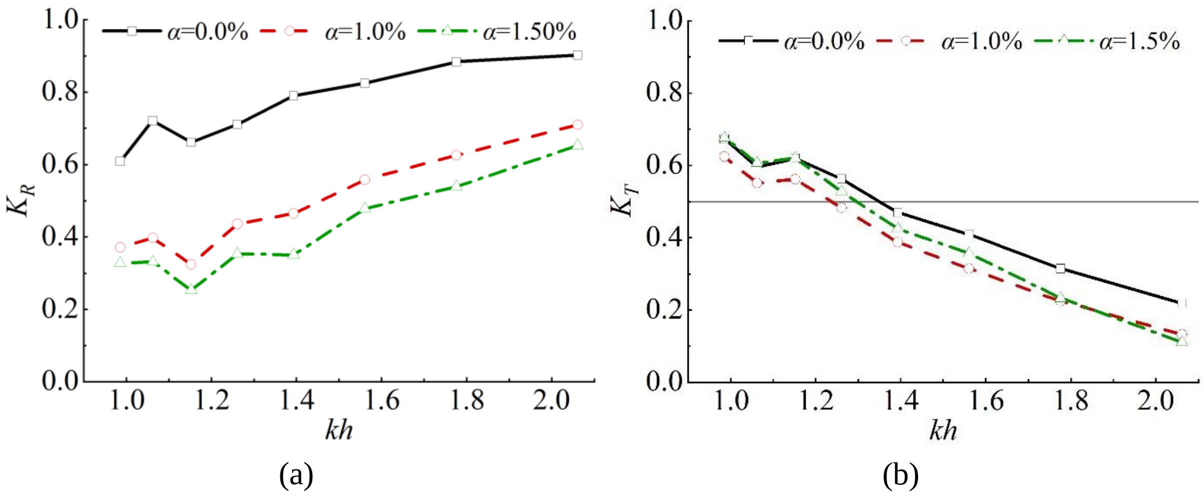

Figure 10. Variations of reflection (a) and transmission coefficient (b) of dual-chamber OWC-breakwater with *kh* in different opening ratios.

The reflection coefficient and the transmission coefficient of the dual-chamber device are shown in Figure 10. The reflection coefficient and transmission coefficient of D2 (α = 1.0%) and D3 (α = 1.5%) are less than that of D1 (α = 0.0%). When wave energy was extracted by the air chambers, both of the reflection coefficient and transmission coefficient will be reduced effectively, and will be beneficial for the function of breakwater. Changes of the opening ratio did not modify the trend of the K_R vs *kh*. In general, the reflection coefficient increases with increasing *kh*, and the adverse trend can be found for the transmission coefficient.

3.2.3 Dissipation coefficient

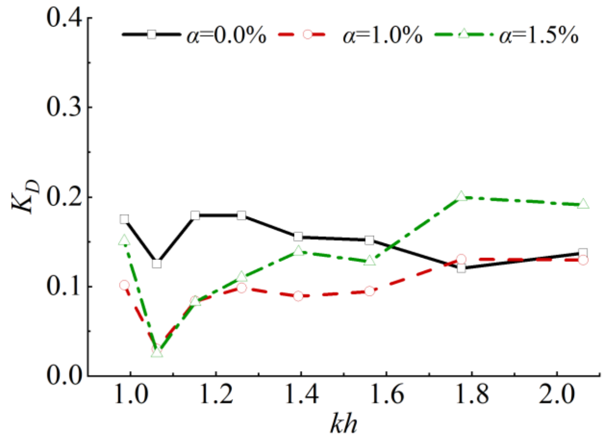

Figure 11. Variations of dissipation coefficient of dual-chamber OWC-breakwater with *kh* in different opening ratios.

The results of dissipation coefficient for dual-chamber device can be found in Figure 11. It can be observed that the dissipated energy for case of α = 0.0% is more dominant for lower frequency region. However, the dissipation coefficient for case of α = 1.5% is relatively larger.

The frequency ranges satisfied the condition of K_T < 0.5 are 1.35 < *kh* <2.06, 1.24 < *kh* <2.06 and 1.30 < *kh* < 2.06 for α = 0.0%, α = 1.0% and α = 1.5%, respectively. And the frequency range for η>0.2 are 0.99 < *kh* <2.06 and 0.99 < *kh* <2.06 for α = 1.0% and α = 1.5%, respectively. Hence, the effective frequency bandwidths corresponding to α = 1.0% and 1.5% are 1.24 < *kh* <2.06 and 1.30 < *kh* <2.06, respectively.

3.3 Hydrodynamic performance of the triple-chamber OWC-breakwater

In this section, the hydrodynamic performance of triple-chamber OWC-breakwater was examined. The incident wave height was fixed as 0.05 m. The wave periods *T* varies from 1.1

s to 1.8 s at interval of 0.1 s. The models of the triple-chamber OWC-breakwater are marked as T1, T2, T3 and T4 (see Tab. 1).

3.3.1 Capture width ratio

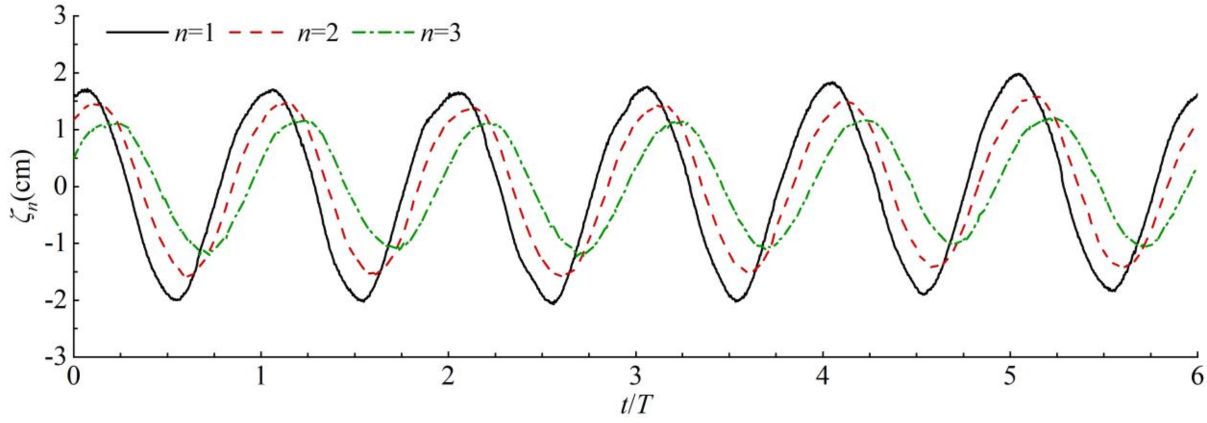

(a)

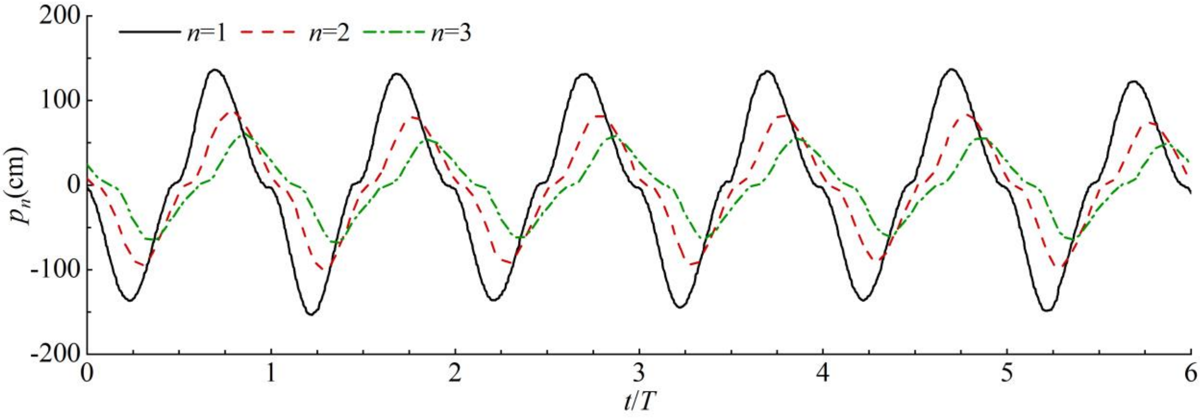

(b)

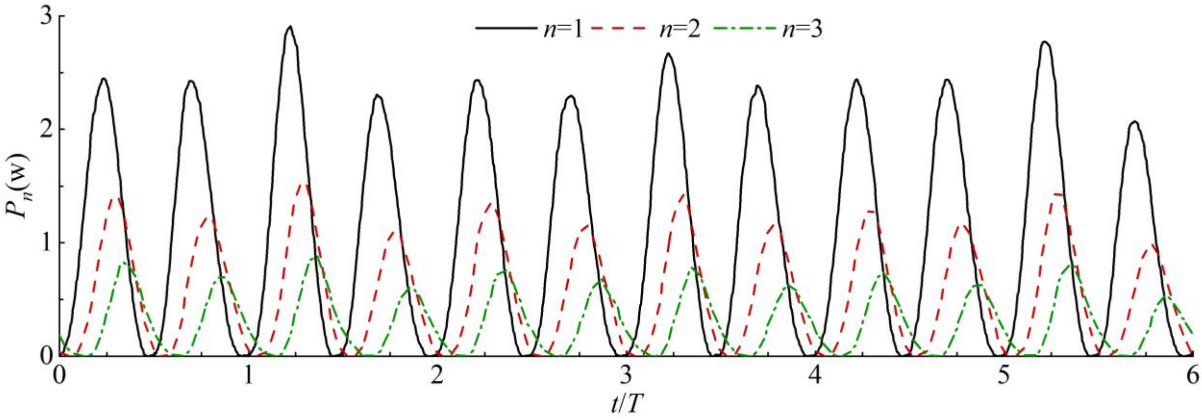

(c)

Figure 12. The time-history series of the free-surface elevation (a), air pressure fluctuation (b) and absorbed power (c) inside each chamber (T2, *kh*= 1.56).

Figure 12(a-c) plot the time-history series of the free surface elevation (WG5, WG6, WG7), air pressure fluctuation and absorbed power inside each chamber for case of kh = 1.56 and H_i = 0.05 m. It was found that there is an obvious phase difference for the three chambers. The peak and valley values of the free surface elevation and air pressure fluctuation exist a 1/4 period difference. Symbolically, ζ_n, p_n and P_n (n = 1, 2 and 3) represent the free surface elevation, air pressure fluctuation and absorbed power inside the front chamber, middle chamber and the rear chamber, respectively.

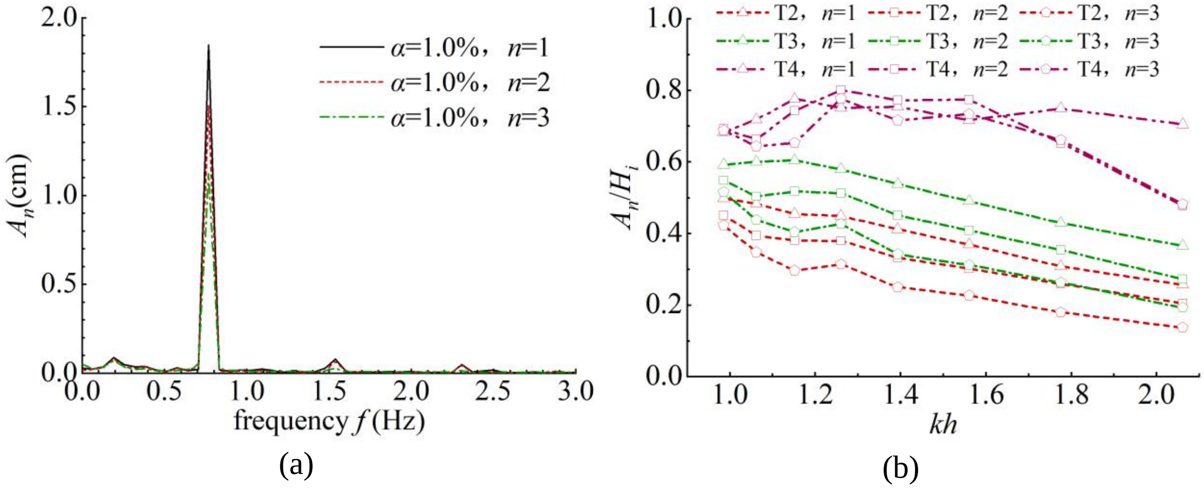

Figure 13. Spectral frequency analysis of the free surface elevation for case of kh =1.56 (a) and variations of the relative wave amplitude A_n/H_i (b)with kh for the triple-chamber OWC-breakwater

The second- and third- order wave amplitude are observed from the frequency spectral analysis shown in Figure 13(a), But they are not dominate values while comparing with the wave amplitude of first-order component. In the following only the first-order wave amplitude was compared.

Figure 13(b) shows that the relative wave amplitude in the chambers for different opening ratios. It can be obtained that the relative wave amplitude increases at each chamber with the increasing opening ratio. For cases of T2 (α = 1.0%) and T3 (α = 1.5%), due to the shadow effect, the relative wave amplitude in the chamber decreases with its location moves the rear side.

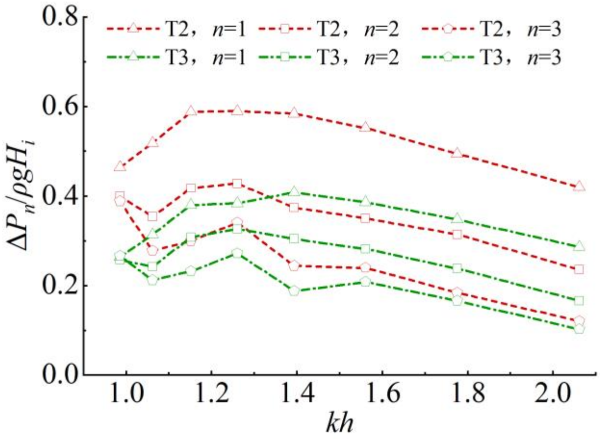

Figure 14. Variations of the relative amplitude of air pressure fluctuation $\Delta P_n/\rho g H_i$ of triple-chamber OWC-breakwater with *kh* in different opening ratios.

The relative amplitude of air pressure fluctuation in each chamber for case of α = 1.0% and 1.5% are shown in Figure 14. For case of T4 (α = 15.8%, fully opened), the relative amplitude of air pressure fluctuation are zero in all the chambers. Therefore, it was decided not plot the results of T4 in Figure 14. The relative amplitude of air pressure fluctuation at each chamber for case of α = 1.0% is greater than that for case of α = 1.5%. The relative amplitude of air pressure fluctuation in the front chamber shows the parabolic trend. Differently, for the relative amplitude of air pressure fluctuation in the middle chamber and rear chamber, there is a valley value at the lower frequency region (i.e., *kh* = 1.06). The locations of the peak value in different chambers are similar.

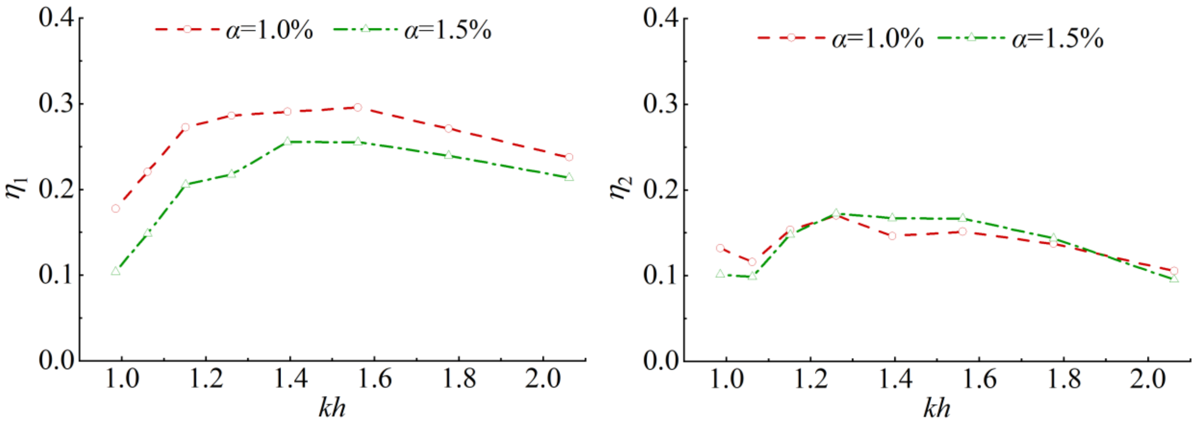

(a) (b)

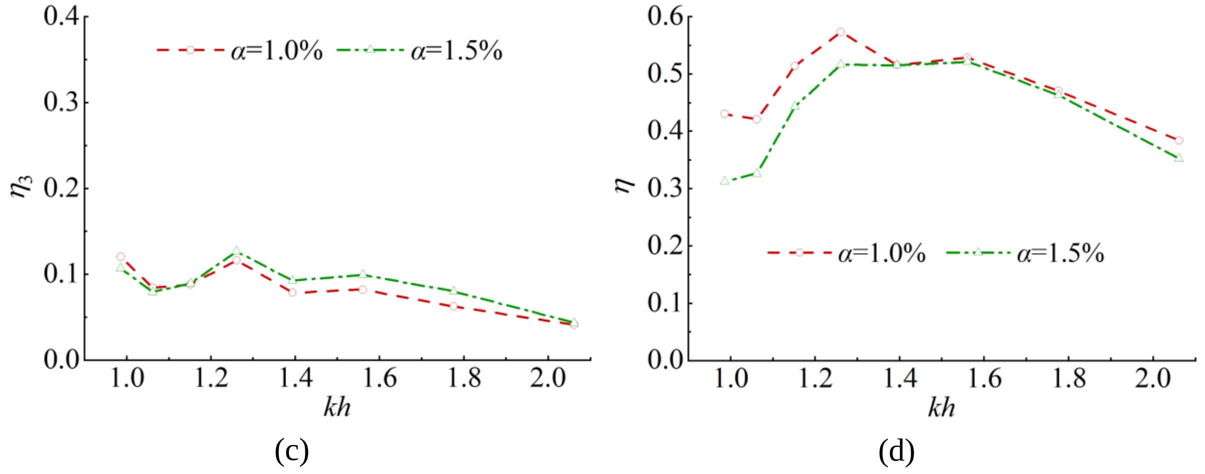

Figure 15. Variations of η_1, η_2, η_3 and η, for the triple-chamber OWC-breakwater with kh in different opening ratios.

The *CWR* in different chambers and the total *CWR* are shown in Figure 15. When the opening ratios are 0% and 15.8%, there are no wave energy extracted. The total *CWR* for case of α = 1.0% is greater than that for case of α = 1.5% over the whole tested frequency region. The maximum *CWR* for case of α = 1.0% and 1.5% are 57.3% and 52.1%, respectively. They are larger than that for the single-chamber OWC-breakwater (43.1% and 38.4%) under the same opening ratio. Refering to Figure 9(d), the maximum *CWR* of dual-chamber OWC-breakwater for case of α= 1.0% and 1.5% are 54.5% and 55.8%, respectively. Overall, the maximum *CWR* of triple-chamber OWC-breakwater is larger than that of single- and dual-chamber system.

For *CWR* of different chambers, the trend against kh are similar to that of the relative amplitude of air pressure fluctuation in Figure 14. But the locations of the peak value for different chambers are different due to the hydrodynamic interactions of each water column.

3.3.2 Reflection coefficient and transmission coefficient

The reflection coefficient and transmission coefficient for the triple-chamber OWC-breakwater are shown in Figure 16. The opening ratio modified the trend of K_R vs kh. For cases of α = 0.0% and 1.0%, the reflection coefficient increases with the increasing wave number. A valley value is found at kh = 1.26 for cases of α = 1.5% and 15.8%. Similar to that for the single-chamber and dual-chamber OWC-breakwaters, the increasing of the opening ratio decreases the reflection coefficient for each fixed wave number. For the tested four cases, the trend of K_T

vs *kh* are similar. Changing the opening ratio of the air chamber did not modify the trend of K_T vs *kh*. But, for a fixed wave number, the opening ratio affect the transmission coefficient, which is reflected in that K_T decreases firstly and then increases with the increasing opening ratio.

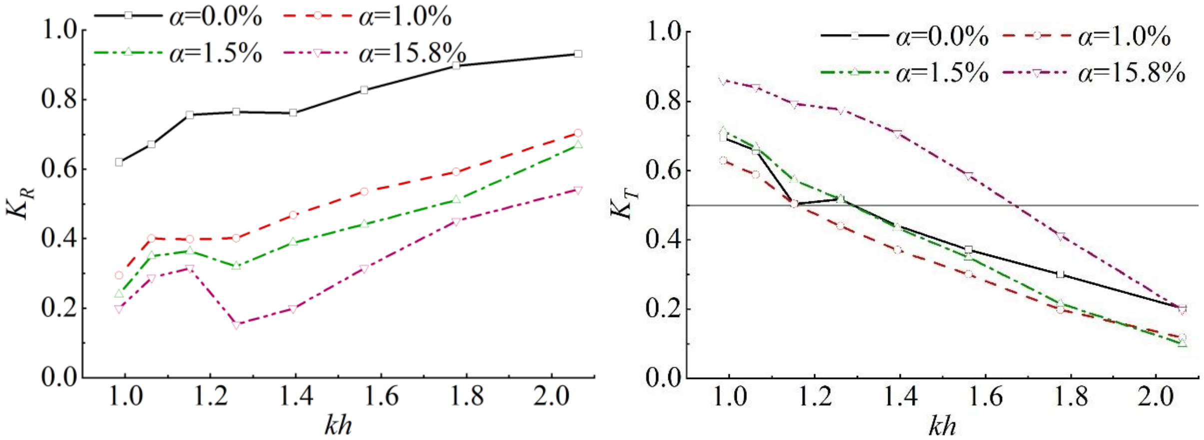

Figure 16. Variations of reflection coefficient (a) and transmission coefficient (b) of triple-chamber OWC-breakwater with *kh* in different opening ratios.

3.3.3 Dissipation coefficient

From Figure 17, we can conclude that the variations of K_D against *kh* for opening ratios of α = 0%, 1.0% and 1.5% are similar to that found in dual-chamber system. The value of K_D for the triple-chamber OWC-breakwater is similar to that of dual-chamber OWC-breakwater, which is less than that of single-chamber OWC-breakwater. The K_D for α = 0%, 1.0% and 1.5% are obviously less than that of 15.8%, especially at the high frequency region. The maximum K_D of the triple-chamber OWC-breakwater for α = 15.8% approaches to 66.7% due to the higher velocity at the tip of the plate.

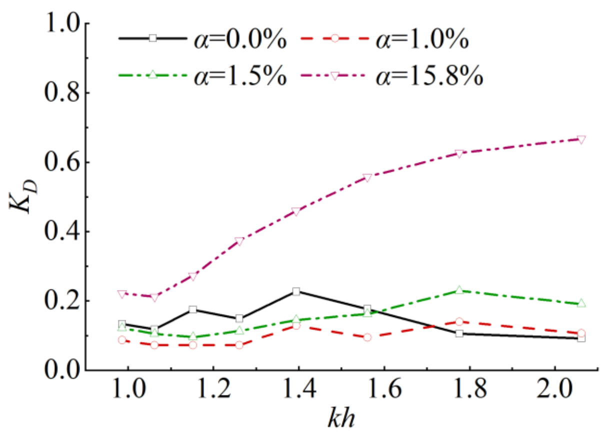

Figure 17. Variations of dissipation coefficient of triple-chamber OWC-breakwater with *kh* in different opening ratios.

From Figure 15(d), we found that the condition of $\eta > 0.2$ can be satisfied over the whole tested frequency region for cases of T2 (α = 1.0%) and T3 (α = 1.5%). The frequency ranges that satisfied $K_T < 0.5$ for cases of T2 and T3 are $1.16 < kh < 2.06$ and $1.29 < kh < 2.06$, respectively. Therefore, the frequency ranges that satisfied both conditions of $K_T < 0.5$ and $\eta > 0.2$ are $1.16 < kh < 2.06$ and $1.29 < kh < 2.06$ for α = 1.0% and 1.5%.

3.4 Effect of wave nonlinearity on the performance of the triple-chamber OWC-breakwater

To investigate the effect of wave nonlinearity, experiments were carried out for fixed parameters of α = 1.0%. The corresponding wave steepness ε (H_i/L) was shown as Table 5.

Table 5 The wave steepness of different cases.

T (s)	1.1	1.2	1.3	1.4	1.5	1.6	1.7	1.8
L (m)	1.83	2.12	2.42	2.71	2.99	3.27	3.55	3.82
ε (H_i=0.05m)	0.027	0.024	0.021	0.018	0.017	0.015	0.014	0.013
ε (H_i=0.075m)	0.041	0.035	0.031	0.028	0.025	0.023	0.021	0.020
ε (H_i=0.10m)	0.055	0.047	0.041	0.037	0.033	0.031	0.028	0.026

3.4.1 Capture width ratio

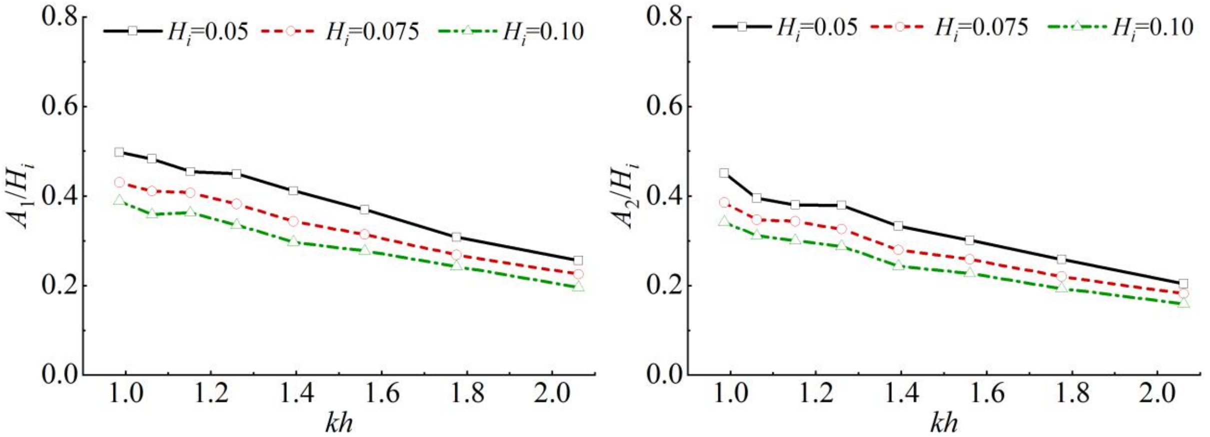

(a) (b)

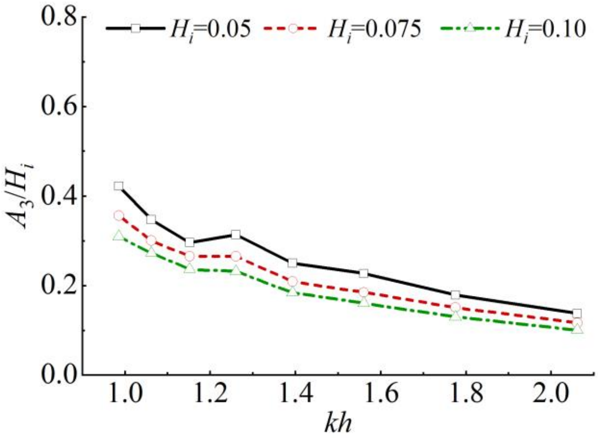

(c)

Figure 18. Variations of the relative wave amplitude A_1/H_i (a), A_2/H_i (b) and A_3/H_i (c) of triple-chamber OWC-breakwater with *kh* in different incident wave heights.

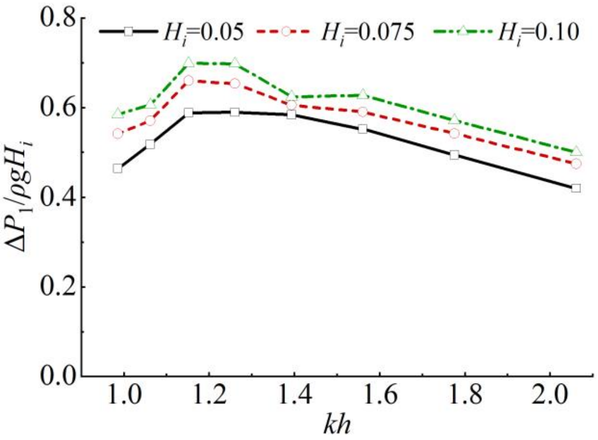

(a)

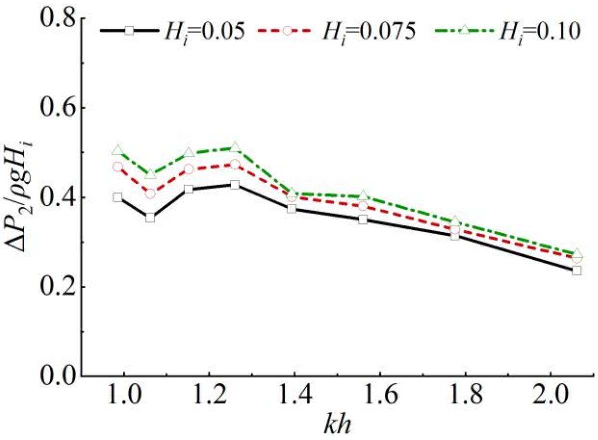

(b)

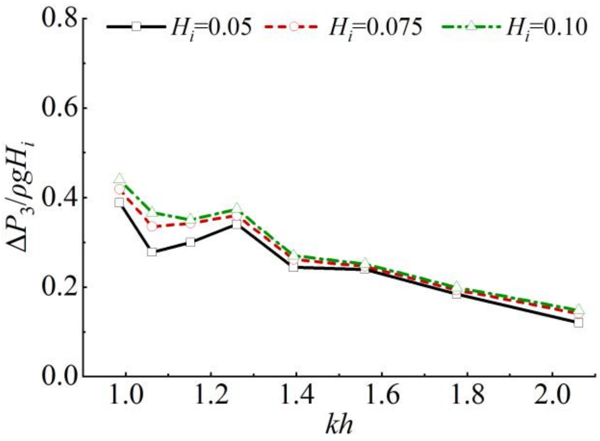

(c)

Figure 19. Variations of the relative amplitude of air pressure fluctuation $\Delta P_1/\rho g H_i$ (a),

$\Delta P_2/\rho g H_i$ (b) and $\Delta P_3/\rho g H_i$ (c) of triple-chamber OWC-breakwater with *kh* in different incident wave heights.

Figure 18(a-c) show relative wave amplitude in different chambers. It can be seen that the wave heights do affect the relative wave amplitude of the three chambers. It mainly reflected in that the dimensionless wave amplitude decreases with the increasing wave nonlinearity. This is due to the viscosity dissipation caused by vortex shedding in case of greater wave amplitude. However, the opposite trend can be found for the relative amplitude of air pressure fluctuation in each chamber in Figure 19(a-c). The pressure fluctuation inside of the chamber is quadratic function of the velocity of the water column inside the chamber [58-59].

The simplified equation of the pressure is shown in Eq. 15 [60], $p(t) = \frac{\rho_a C_f}{2}\left|\bar{u}(t)\right|\bar{u}(t)$, where p (t) is the pressure fluctuation inside the OWC chamber, ρ_a is the air density, C_f is the quadratic loss coefficient and $\bar{u}(t)$ is the spatially-averaged surface velocity.

However, the denominator of the dimensionless formula $\Delta P_n/\rho g H_i$ is the linear function of H_i. Hence, the greater wave nonlinearity leads to the greater dimensionless relative amplitude of air pressure fluctuation in Figure 19, the viscosity dissipation is also one of the reasons.

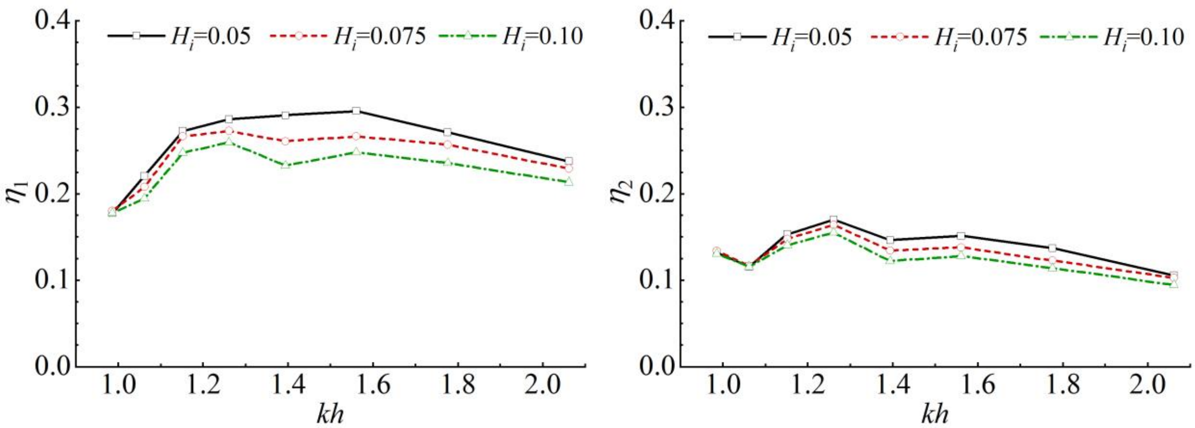

(a) (b)

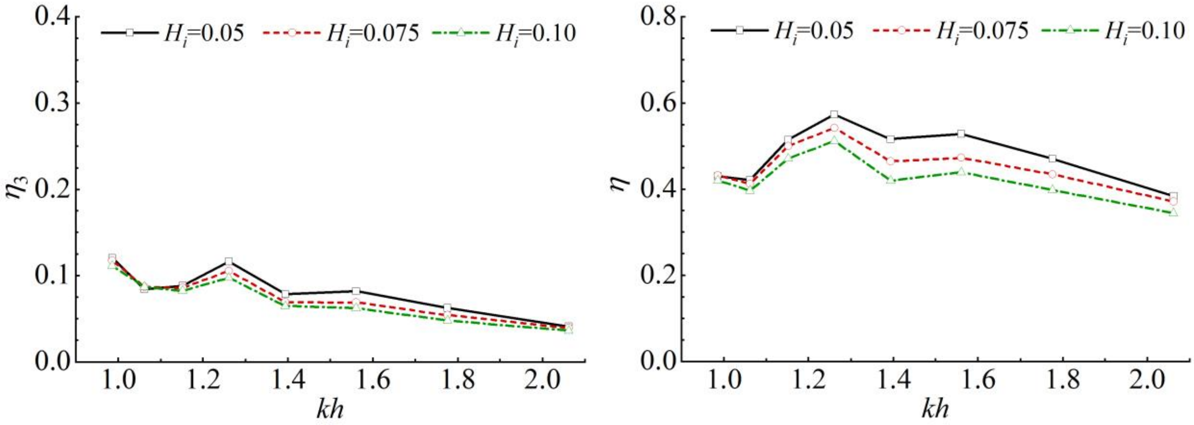

(c) (d)

Figure 20. Variations of η_1 (a), η_2 (b), η_3 (c) and the total *CWR* η (d) of triple-chamber OWC-breakwater with *kh* in different incident wave heights.

The *CWR* of each chamber and the total *CWR* are shown in Figure 20. The maximum *CWR* of triple-chamber OWC-breakwater are 57.3%, 54.2% and 51.2% when the incident wave heights are 0.05m, 0.075m and 0.10m, respectively. The increasing of wave nonlinearity decreases the *CWR* of the device, which is similar to the trend of the relative wave amplitude against the relative amplitude of air pressure fluctuation. Similarly, this trend can be explained by viscous dissipation. Also, for different incident wave heights, the *CWR* of the chamber in the leeside is smaller than that in the weather side due to the shadow effect. Moreover, slight influence of the wave nonlinearity can be found for the chambers in the leeside.

By comparing with the *CWR* of different chambers, we found that there exists a valley value at *kh* = 1.06 for the *CWR* of chamber in middle section and in the leeside. However, this phenomenon is absent for the *CWR* of the chamber in the weather side. The aforementioned valley value lead to the valley value at similar location for the total *CWR*. Correspondingly, the valley value can also be found for the relative amplitude of air pressure fluctuation in Figure 19(b) and (c). But, the relative amplitude of air pressure fluctuation of the chamber in the weather side does not experience this valley value. When we recall the variations of relative wave amplitude in the chambers, the valley value is absent for the relative wave amplitude in the front chamber.

3.4.2 Reflection coefficient and transmission coefficient

The results of the reflection coefficient and transmission coefficient of the OWC-breakwater with triple-chamber are shown in Figure 21.

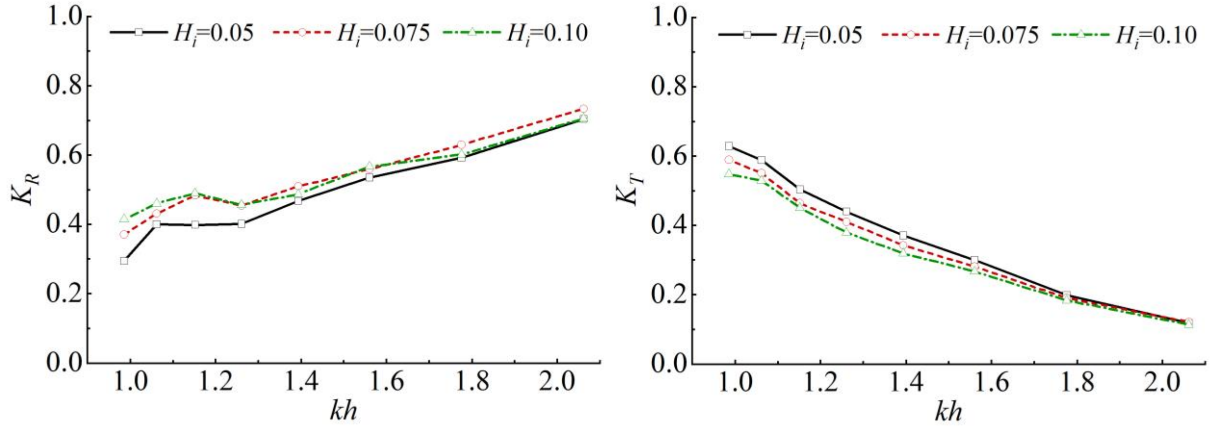

(a) (b)

Figure 21. Variations of reflection coefficient (a) and transmission coefficient (b) of triple-chamber OWC-breakwater with *kh* in different incident wave heights.

Generally, the trend of K_R and K_T is not affected by the dimensionless wave number nor by the wave nonlinearity. But the wave nonlinearity affects the reflection transmission coefficient significantly for fixed wave period at lower frequency (i.e., $0.99 < kh < 1.26$). Generally, the reflection coefficient increases and the transmission coefficient decreases with the increasing of wave nonlinearity.

3.4.3 Dissipation coefficient

Figure 22 shows the results of dissipation coefficient K_D for different incident wave heights. Wave nonlinearity does not modify the trend of K_D vs *kh*. The dissipation coefficient increases firstly and then decreases with increasing *kh*, and the peak value of K_D appears at the middle frequency region. The wave nonlinearity affects K_D slightly at the lower frequency region (i.e., $0.99 < kh < 1.26$). Comparatively, obvious influences can be found at the rest frequency region (i.e., $1.26 < kh < 2.06$), where K_D increases with the increasing wave nonlinearity.

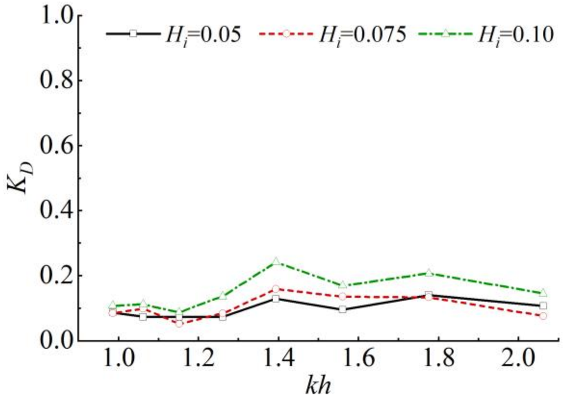

Figure 22. Variations of dissipation coefficient of triple-chamber OWC-breakwater with *kh* in different incident wave heights.

For the tested incident wave heights, the *CWR* for each wave period is greater than 0.2 for α = 1.0%. From Figure 21(b), we found that the frequency range for K_T <0.5 is larger when H_i = 0.10m. The corresponding frequency ranges are 1.16 < *kh* < 2.06, 1.11 < *kh* < 2.06 and 1.10 < *kh* < 2.06 when the incident wave heights are 0.05 m, 0.075 m and 0.10 m. When we consider the *CWR* and transmission coefficient together, though the total *CWR* decreases, the effective frequency bandwidth increases slightly due to the wave nonlinearity.

3.5 Discussions on wave energy extraction performance and wave attenuation performance of OWC-breakwaters

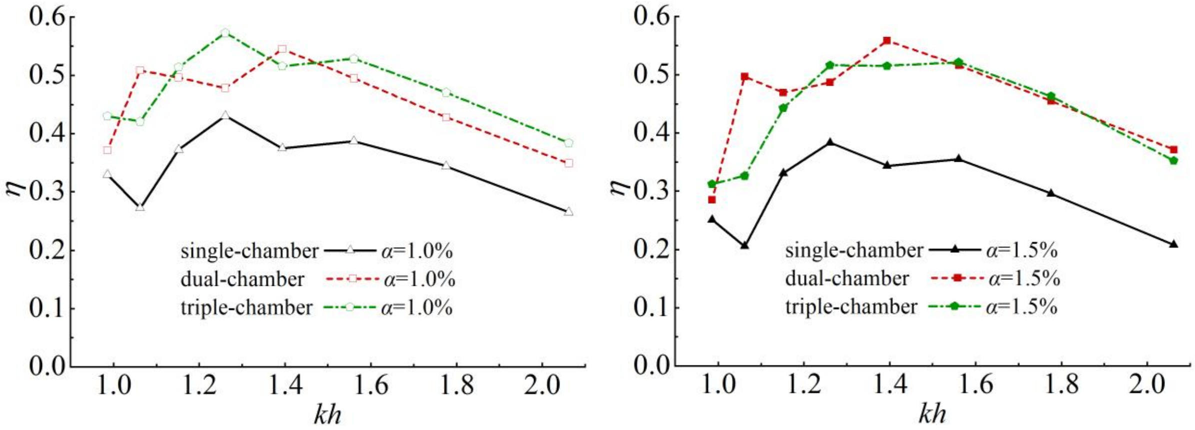

(a) (b)

Figure 23. Results of total CWR η for case of α = 1.0% (a) and 1.5% (b)

The total capture width ratio of OWC-breakwaters with different chamber numbers are shown in Figure 23. Form Figure 23, it was found that the *CWR* of the dual-chamber and triple-chamber OWC-breakwaters, are observably superior to single-chamber OWC-breakwater over the whole frequency region for α = 1.0% and 1.5%. Also, for the current set-up, we found that the total *CWR* approaches to a convergence value with increasing chamber number. The comparisons prove that, under the premise of same total water column volume, the multi-chamber OWC-breakwater performs better than that of the counterpart with single-chamber.

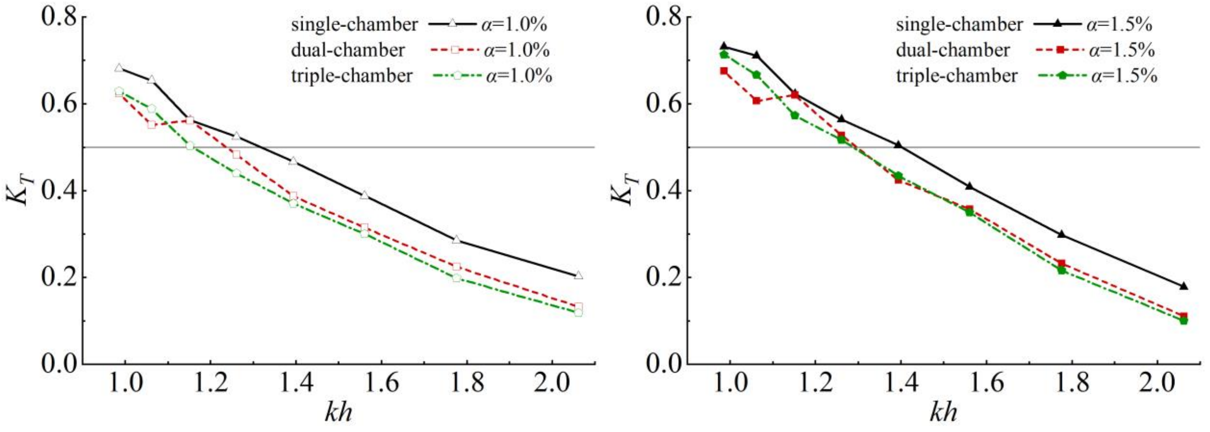

(a) (b)

Figure 24. Results of transmission coefficient for case of α = 1.0% (a) and 1.5% (b)

The transmission coefficient of OWC-breakwaters are shown in Figure 24. Form Figure 24, it was found that the transmission coefficient of the multi-chamber OWC-breakwater is less than that of the single-chamber OWC-breakwater.

From the direct comparisons of the *CWR* and transmission coefficient of the device with multiple chambers, it can be found that the effective frequency bandwidth of the OWC-breakwaters with dual- and triple-chamber are wider than that of the single-chamber device. These advantages are beneficial for the floating OWC-breakwater as breakwaters. However, comparing the effective frequency bandwidth of the dual- and triple-chamber devices, the present results suggest no obvious advantages for the triple-chamber device.

For the breakwater it is interesting to broaden its frequency range for K_T < 0.5 to improve the wave attenuation performance in the floating breakwater in longer waves. In this study, the frequency ranges of triple-chamber OWC-breakwater with satisfactory wave attenuation performance for 1.0% and 1.5% are 1.16 < *kh* < 2.06 and 1.29 < *kh* < 2.06. More case studies, comparisons and optimizations are worthy exploring the advantages of the multi-chamber OWC-breakwater.

4 Conclusions

In this study, the hydrodynamic performance of OWC-breakwaters with single-chamber, dual-chamber and triple-chamber were investigated thoroughly via a series of experiments. The principle is that the total water column volume of the chamber for different cases were kept the same. An orifice was used to model the PTO damping. Considering that the OWC-breakwater includes the function of wave energy extraction and breakwater simultaneously, we focus on the *CWR*, reflection coefficient, transmission coefficient, dissipation coefficient and the effective frequency bandwidth. Besides, we emphasized the comparisons of the three kinds of devices.

1) Comparisons of the three OWC-breakwaters showed that the energy extraction performance for the devices with triple-chamber and dual-chamber are better than that for the single-chamber device due to the hydrodynamic interactions of different water columns. Under the premise of the same opening ratio (i.e., 1.0%), the maximum efficiency of triple-chamber device is slightly superior to that of the dual-chamber OWC-breakwater. Due to the shadow effect, the *CWR* at each chamber decrease with its location moves to the leeside of the device.

2) The transmission coefficient in the lower frequency for the device with triple-chamber is less than that of the dual-chamber and single-chamber OWC-breakwaters. That is to say, the wave attenuation performance of the triple-chamber is better. The OWC-breakwater with triple-chamber has a wider effective frequency bandwidth for $\eta > 0.2$ and $K_T < 0.5$.The corresponding frequency range is $1.16 < kh < 2.06$ and $1.29 < kh < 2.06$ when the opening ratio α is 1.0% and 1.5%. This is beneficial for such kind of device to act as dual role of wave energy converter and breakwater.

3) Due to the fact that the multi-chamber OWC-breakwater possesses more effective wave energy extraction, the dissipation coefficient is relatively smaller than that of the single-chamber device with the same opening ratio.

4) Wave nonlinearity plays an important role while evaluating the performance of the OWC-breakwater with triple-chamber. The total efficiency and the transmission coefficient decrease with the increasing of wave nonlinearity, but the effective frequency bandwidth increases slightly.

The hydrodynamic analysis on the OWC-breakwaters with single-chamber, dual-chamber and triple-chamber and the direct comparisons are helpful to in-depth research on hydrodynamic mechanism of the device with multi-chamber. And the performance of the wave energy converters in chaotic sea state is worthy to be investigated.

The hydrodynamic interactions of the multiple water columns are worthy to be further investigated. The formula we used to evaluate the natural frequency of the columns is originated from case of single-chamber in isolation [46]. The added mass of each chamber is different to that of the isolated case due to the hydrodynamic interactions of different columns, which may affect the natural frequency of the water columns. This may lead to the modifications of formula in case of multi-chamber OWC-breakwater. This interesting topic is worthy to be investigated.

In addition, experiments were conducted under regular waves in this study. It is well-known that the realistic deployment sites have irregular waves. The advantages of the multi-chamber device shall be examined in realistic wave conditions. Also, the survivability in severe sea conditions is worthy to be investigated in the future.

Acknowledgements

Key Program for International Scientific and Technological Innovation Cooperation between Governments(2019YFE0102500); Open Foundation of State Key Laboratory of Coastal and Offshore Engineering, China (LP1927); National Key Research and Development Project of China(2019YFB1504403); National Natural Science Foundation of China (51509056); China Postdoctoral Science Foundation funded project(2019M661257). Special thanks go to TUS-ORE Catapult for their valuable contributions.

References:

[1] Liu J. China's renewable energy law and policy: A critical review. Renewable and Sustainable Energy Reviews. 2019;99:212-9.

[2] Melikoglu M. Current status and future of ocean energy sources: A global review. Ocean Eng. 2018;148:563-73.

[3] Neill SP, Hashemi MR. Chapter 5 - Wave Energy. In: S. P. Neill, M. R. Hashemi, ^editors. Fundamentals of Ocean Renewable Energy: Academic Press; 2018. p. 107-40.

[4] Falcão AFDO. Wave energy utilization: A review of the technologies. Renewable and Sustainable Energy Reviews. 2010;14:899-918.

[5] Falcão AFO, Henriques JCC. Oscillating-water-column wave energy converters and air turbines: A review.

Renew Energ. 2016;85:1391-424.
[6] EVANS DV. The Oscillating Water Column Wave-energy Device. Ima J Appl Math. 1978;22:423-33.
[7] He F, Huang Z. Hydrodynamic performance of pile-supported OWC-type structures as breakwaters: An experimental study. Ocean Eng. 2014;88:618-26.
[8] Ning D, Wang R, Zou Q, Teng B. An experimental investigation of hydrodynamics of a fixed OWC Wave Energy Converter. Appl Energ. 2016;168:636-48.
[9] Kamath A, Bihs H, Arntsen ØA. Numerical modeling of power take-off damping in an Oscillating Water Column device. International Journal of Marine Energy. 2015;10:1-16.
[10] Luo Y, Nader J, Cooper P, Zhu S. Nonlinear 2D analysis of the efficiency of fixed Oscillating Water Column wave energy converters. Renew Energ. 2014;64:255-65.
[11] He F, Zhang H, Zhao J, Zheng S, Iglesias G. Hydrodynamic performance of a pile-supported OWC breakwater: An analytical study. Appl Ocean Res. 2019;88:326-40.
[12] Sarmento AJNA, Falcão AFDO. Wave generation by an oscillating surface-pressure and its application in wave-energy extraction. J Fluid Mech. 1985;150:467-85.
[13] Singh U, Abdussamie N, Hore J. Hydrodynamic performance of a floating offshore OWC wave energy converter: An experimental study. Renewable and Sustainable Energy Reviews. 2020;117:109501.
[14] Zabala I, Henriques JCC, Blanco JM, Gomez A, Gato LMC, Bidaguren I, et al. Wave-induced real-fluid effects in marine energy converters: Review and application to OWC devices. Renewable and Sustainable Energy Reviews. 2019;111:535-49.
[15] Torre-Enciso Y, Ortubia I, López De Aguileta LI, Marqués J. Mutriku Wave Power Plant: From the Thinking out to the Reality2009.
[16] Arena F, Romolo A, Malara G, Fiamma V, Laface V. Response of the U-OWC Prototype Installed in the Civitavecchia Harbour.2018.
[17] Arena F, Romolo A, Malara G, Fiamma V, Laface V. The First Full Operative U-OWC Plants in the Port of Civitavecchia.2017.
[18] Mustapa MA, Yaakob OB, Ahmed YM, Rheem C, Koh KK, Adnan FA. Wave energy device and breakwater integration: A review. Renewable and Sustainable Energy Reviews. 2017;77:43-58.
[19] Zhao XL, Ning DZ, Zou QP, Qiao DS, Cai SQ. Hybrid floating breakwater-WEC system: A review. Ocean Eng. 2019;186:106126.
[20] Doyle S, Aggidis GA. Development of multi-oscillating water columns as wave energy converters. Renewable and Sustainable Energy Reviews. 2019;107:75-86.
[21] Shalby M, Dorrell DG, Walker P. Multi‐chamber oscillating water column wave energy converters and air turbines: A review. Int J Energ Res. 2019;43:681-96.
[22] Hsieh M, Lin I, Dorrell DG, Hsieh M, Lin C. Development of a Wave Energy Converter Using a Two Chamber Oscillating Water Column. Ieee T Sustain Energ. 2012;3:482-97.
[23] Martinelli L, Pezzutto P, Ruol P. Experimentally Based Model to Size the Geometry of a New OWC Device, with Reference to the Mediterranean Sea Wave Environment. Energies. 2013;6:4696-720.
[24] Rezanejad K, Bhattacharjee J, Guedes Soares C. Analytical and numerical study of dual-chamber oscillating water columns on stepped bottom. Renew Energ. 2015;75:272-82.
[25] Ning D, Wang R, Zhang C. Numerical Simulation of a Dual-Chamber Oscillating Water Column Wave Energy Converter. Sustainability-Basel. 2017;9:1599.

[26] Ning D, Wang R, Chen L, Sun K. Experimental investigation of a land-based dual-chamber OWC wave energy converter. Renewable and Sustainable Energy Reviews. 2019;105:48-60.

[27] Iturrioz A, Guanche R, Armesto JA, Alves MA, Vidal C, Losada IJ. Time-domain modeling of a fixed detached oscillating water column towards a floating multi-chamber device. Ocean Eng. 2014;76:65-74.

[28] He F, Huang Z, Law AW. An experimental study of a floating breakwater with asymmetric pneumatic chambers for wave energy extraction. Appl Energ. 2013;106:222-31.

[29] He F, Leng J, Zhao X. An experimental investigation into the wave power extraction of a floating box-type breakwater with dual pneumatic chambers. Appl Ocean Res. 2017;67:21-30.

[30] Howe D, Nader J, Macfarlane G. Experimental investigation of multiple Oscillating Water Column Wave Energy Converters integrated in a floating breakwater: Energy extraction performance. Appl Ocean Res. 2020;97:102086.

[31] Elhanafi A, Macfarlane G, Ning D. Hydrodynamic performance of single‐chamber and dual‐chamber offshore‐stationary Oscillating Water Column devices using CFD. Appl Energ. 2018;228:82-96.

[32] Ning D, Zhou Y, Mayon R, Johanning L. Experimental investigation on the hydrodynamic performance of a cylindrical dual-chamber Oscillating Water Column device. Appl Energ. 2020;260:114252.

[33] Ning DZ, Zhou Y, Mayon R, Johanning L. Experimental investigation on the hydrodynamic performance of a cylindrical dual-chamber Oscillating Water Column device. Appl Energ. 2020;260.

[34] Shalby M, Walker P, Dorrell DG. Modelling of the multi-chamber oscillating water column in regular waves at model scale. Energy Procedia. 2017;136:316-22.

[35] Shalby M, Elhanafi A, Walker P, Dorrell DG. CFD modelling of a small‐scale fixed multi‐chamber OWC device. Appl Ocean Res. 2019;88:37-47.

[36] Elhanafi A, Macfarlane G, Ning D. Hydrodynamic performance of single‐chamber and dual‐chamber offshore‐stationary Oscillating Water Column devices using CFD. Appl Energ. 2018;228:82-96.

[37] Thiruvenkatasamy K, Neelamani S. On the efficiency of wave energy caissons in array. Appl Ocean Res. 1997;19:61-72.

[38] Goda Y, Yasumasa S. Estimation of incident and reflected waves in random wave experiments.1976.

[39] Mei CC, Stiassnie MA, Yue DK. Theory and Applications of Ocean Surface Waves: World Scientific; 2005.

[40] Fossa M, Guglielmini G. Pressure drop and void fraction profiles during horizontal flow through thin and thick orifices. Exp Therm Fluid Sci. 2002;26:513-23.

[41] ITTC. Recommended Procedures and Guidelines: Practical Guidelines for Ship CFD. International Towing Tank Conference. 2011:1-18.

[42] CD-Adapco. User Guide STAR-CCM+ Version 10.02. User Guide STAR-CCM+ Version 10.02. 2015.

[43] Falcão AFO, Henriques JCC. Oscillating-water-column wave energy converters and air turbines: A review. Renew Energ. 2016;85:1391-424.

[44] Delmonte N, Barater D, Giuliani F, Cova P, Buticchi G. Oscillating water column power conversion: A technology review.: IEEE 2014. p. 1852-9.

[45] Heath TV. A review of oscillating water columns. Philosophical Transactions of the Royal Society A: Mathematical, Physical and Engineering Sciences. 2012;370:235-45.

[46] Veer RV, Tholen HJ. Added resistance of moonpools in calm water. Proceedings of the International Conference on Offshore Mechanics and Arctic Engineering - OMAE2008. p. 153-62.

[47] Sarmento AJNA. Wave flume experiments on two-dimensional oscillating water column wave energy devices.

Exp Fluids. 1992;12-12:286-92.
[48] Ning D, Zhao X, Göteman M, Kang H. Hydrodynamic performance of a pile-restrained WEC-type floating breakwater: An experimental study. Renew Energ. 2016;95:531-41.
[49] Ning D, Wang R, Chen L, Sun K. Experimental investigation of a land-based dual-chamber OWC wave energy converter. Renewable and Sustainable Energy Reviews. 2019;105:48-60.
[50] Ning D, Zhao X, Zhao M, Hann M, Kang H. Analytical investigation of hydrodynamic performance of a dual pontoon WEC-type breakwater. Appl Ocean Res. 2017;65:102-11.
[51] Ning DZ, Wang RQ, Chen LF, Sun K. Experimental investigation of a land-based dual-chamber OWC wave energy converter. Renewable and Sustainable Energy Reviews. 2019;105:48-60.
[52] Li M, Zhang L, Zhao X, Geng J. Experimental investigation on hydrodynamic performance of dual-chambers OWC device. Ocean Engineering Equipment and Technology. 2019;6:484-8. (In Chinese)
[53] Zhao XL, Ning DZ, Zou QP, Qiao DS, Cai SQ. Hybrid floating breakwater-WEC system: A review. Ocean Eng. 2019;186.
[54] Mustapa MA, Yaakob OB, Ahmed YM, Rheem CK, Koh KK, Adnan FA. Wave energy device and breakwater integration: A review. Renewable and Sustainable Energy Reviews. 2017;77:43-58.
[55] He F, Huang Z. Hydrodynamic performance of pile-supported OWC-type structures as breakwaters: An experimental study. Ocean Eng. 2014;88:618-26.
[56] Koutandos E, Prinos P, Gironella X. Floating breakwaters under regular and irregular wave forcing: reflection and transmission characteristics. J Hydraul Res. 2005;43:174-88.
[57] Michailides C, Angelides DC. Modeling of energy extraction and behavior of a Flexible Floating Breakwater. Appl Ocean Res. 2012;35:77-94.
[58] Huang Z, Li Y, Liu Y. Hydraulic performance and wave loadings of perforated/slotted coastal structures: a review. Ocean Eng. 2011;38.
[59] Mei CC, Liu PL, Ippen AT. Quadratic loss and scattering of long waves. Journal of the Waterways, Harbors and Coastal Engineering Division. 1974;100.
[60] He F, Huang Z. Characteristics of orifices for modeling nonlinear power take-off in wave-flume tests of oscillating water column devices. Journal of Zhejiang University: Science A. 2017;18:329-45.

Highlights

- ✓ Hydrodynamic performance of the multi-chamber OWC-breakwater is investigated experimentally.
- ✓ Thorough comparisons of the single-, dual- and triple-chamber OWC-breakwater are conducted.
- ✓ The wave attenuation performance of the triple-chamber OWC-breakwater is slightly superior to that of the single- and dual-chamber OWC-breakwater.
- ✓ Wave nonlinearity affects the hydrodynamic performance of the triple-chamber OWC-breakwater.